Journal of
Materials Chemistry B

PAPER

View Article Online
View Journal | View Issue

Cite this: *J. Mater. Chem. B*, 2016, 4, 2179

Conjugation of thiol-terminated molecules to ultrasmall 2 nm-gold nanoparticles leads to remarkably complex ^{1}H-NMR spectra

Benjamin Schuetze,[a] Christian Mayer,[b] Kateryna Loza,[a] Martin Gocyla,[c] M. Heggen[c] and Matthias Epple*[a]

Received 20th November 2015,
Accepted 23rd February 2016

DOI: 10.1039/c5tb02443a

www.rsc.org/MaterialsB

Gold nanoparticles, functionalized by aliphatic and aromatic mercapto-functionalized carboxylic acids and by two small peptides (CG and CGGRGD), respectively, were synthesized by the reduction of $HAuCl_4$ with $NaBH_4$ in the presence of the above ligands. After purification by centrifugation or filtration and redispersion, the dispersed nanoparticles were analysed by differential centrifugal sedimentation (DCS), high-resolution transmission electron microscopy (HRTEM), and a variety of NMR spectroscopic techniques: ^{1}H-NMR, ^{1}H,^{1}H-COSY and ^{1}H-DOSY. The hydrodynamic diameter of the particles was between 1.8 and 4.4 nm, as determined by DOSY, in good agreement with the DCS and HRTEM results. Diffusion ordered spectroscopy (DOSY) turned out to be a valuable and non-destructive tool to determine the hydrodynamic diameter of dispersed nanoparticles and to control the purity of the final particles. The coordination of the organic molecules to the gold nanoparticles resulted in distinct and complex changes in the ^{1}H-NMR spectra. These were only partially explainable but clearly caused by the vicinity of the molecules to the gold nanoparticle.

Introduction

Gold nanoparticles find wide application in chemistry and physics, especially in nanomedicine.[1] Typically, they are prepared by the reduction of gold salts in water, followed by functionalization to terminate the particle growth and to achieve a colloidal stabilization.[2–6] Thiol-terminated ligands are standard compounds for this purpose because the gold–sulphur interaction leads to a strong covalent bond.[7] If bifunctional thiols are applied, they offer the possibility for further covalent functionalization, *e.g.* for application in nanomedicine.[3,4,8–10] A physical method to prepare both "naked" and functionalized gold nanoparticles is laser ablation in liquids.[11,12]

The ultrastructure of such functionalized nanoparticles is typically probed using transmission electron microscopy (giving information on the metallic core) and UV spectroscopy (giving information on excited electrons due to the size quantization effect and surface plasmons). Only little is known on the nature of the gold–ligand interaction and the state of the organic molecule on the surface.

NMR spectroscopy is a most valuable tool in chemistry, but it has only seldom been applied to metallic nanoparticles because the vicinity of the metallic particle strongly distorts the spectrum.[13–22] Therefore, the ligands are sometimes removed from the particles and then analysed separately.[23] Solid-state NMR spectroscopy has its limitations for the analysis of nanoparticles because a minimum amount of material is required and because ^{1}H-NMR spectroscopy is usually not possible in the solid state. However, if the particles are small enough, solution NMR spectra with reasonable quality can be obtained.[20] Especially gold clusters can give detailed insight, as Song *et al.* have shown earlier with thiol-functionalized gold nanoclusters in organic solvents.[17]

In addition, diffusion ordered spectroscopy (DOSY) is a valuable tool to determine the hydrodynamic radius of molecules in solution. This can be transposed to nanoparticles, provided that they are small enough as it was recently shown for gold clusters.[24] DOSY can also be used to confirm that different chemical species are located on the same nanoparticle with the same diffusion coefficient.

Here, we demonstrate how a series of well-defined ultrasmall gold nanoparticles was prepared, functionalized with a number of thiol-containing ligands, and analysed by high-end solution NMR spectroscopy. The results underscore the possibilities, but also show the limitations of this method in the analysis of nanoparticles.

[a] *Inorganic Chemistry and Center for Nanointegration Duisburg-Essen (CeNIDE), Universitaetsstr. 5-7, 45117 Essen, Germany. E-mail: matthias.epple@uni-due.de*
[b] *Physical Chemistry and Center for Nanointegration Duisburg-Essen (CeNIDE), Universitaetsstr. 5-7, 45117 Essen, Germany*
[c] *Ernst Ruska-Center and Peter Gruenberg Institute, Forschungszentrum Juelich GmbH, 52425 Juelich, Germany*

Experimental

Synthesis of nanoparticles

2-Mercaptoacetic acid (purity >99%), 3-mercaptopropionic acid (purity >99%), 6-mercaptohexanoic acid (purity 90%), 2-mercaptobenzoic acid (purity 97%), 3-mercaptobenzoic acid (purity 95%), 4-mercaptobenzoic acid (purity 99%), the dipeptide CG (purity >85%), and sodium borohydride (purity >96%) were obtained from Sigma-Aldrich. The hexapeptide CGGRGD was obtained from ThermoFisher Scientific (purity 98%). All ligands were used as received without further purification. Ultrapure water (Purelab ultra instrument from ELGA) was used for all preparations.

$HAuCl_4$ was prepared by dissolution of elemental gold in *aqua regia*. $HAuCl_4$ (5 μmol) was dissolved in 20 mL degassed water, and the corresponding mercaptocarboxylic acid (15 μmol dissolved in 100 μL water) was added under stirring. Then $NaBH_4$ (20 μmol dissolved in 100 μL water) was added as a reducing agent. The mixture was stirred for another 5 min and centrifuged at 3500 rpm. Under these conditions (pH between 1 and 2), the particles were agglomerated due to protonation of the carboxy groups (causing the absence of electrostatic repulsion) and were collected by centrifugation. The supernatant was removed and the nanoparticles were easily redispersed by shaking in 15 mL ultrapure water and purified by centrifugation two more times. An excess of (dissolved) ligand was removed by extraction of the particle dispersion (in 10 mL ultrapure water) twice with the same volume of diethyl ether. This washing step was important to remove disulphide compounds that can form during the reaction by reduction, especially in the case of the aromatic compounds. After centrifugation, the samples were dried in a vacuum to remove the excess of diethyl ether and water.

Characterization techniques

Differential centrifugal sedimentation (DCS) was performed with a CPS Instruments Disc Centrifuge DC 24 000 at 24 000 rpm. Two sucrose solutions (8 wt% and 24 wt%) were used as density gradients which were supplemented with 0.5 mL *N*-dodecane as a stabilizing agent. The calibration standard was a poly(vinyl chloride) (PVC) latex in water with a particle size of 476 nm obtained from CPS instruments. Calibration was carried out prior to each run. A sample volume of 100 μL was used for each experiment.

High-resolution imaging was performed using an aberration-corrected FEI Titan transmission electron microscope operated at 300 kV. The nanoparticles were dispersed on ultra-thin carbon films supported on lacey carbon film Cu-grids (Ted Pella, Inc.). The particle size was estimated by measuring the maximum diameter of 35 particles and accumulating the data into a histogram.

About 1 mg of each sample was dissolved in 300 μL D_2O. 100 μL of a 1 M solution of ND_3 in D_2O was added to increase the pH to ensure electrostatic stabilization by deprotonation of the carboxy groups. ^{1}H-NMR spectra were recorded using a Bruker DPX 300 MHz spectrometer and a Bruker-Avance III 600 MHz spectrometer equipped with a Prodigy cryo probe head. ^{1}H,^{1}H-COSY spectra were recorded using a Bruker-Avance III 600 MHz spectrometer. Diffusion ordered NMR spectroscopy (DOSY) measurements were performed using a Bruker Avance 400 MHz spectrometer with a direct probe at 298 K. A 2D-stimulated echo sequence (diffSte) was used for the diffusion experiments with a trapezoid-shape pulsed gradient duration δ of 500 μs incremented from 15 to 340 G cm^{-1} in 32 steps. The diffusion time Δ was 50 ms. The diffusion coefficients were computed with the T_1/T_2 relaxation module of the TopSpin 3.0 software. The measured diffusion coefficient D and the viscosity η of 1.0963 mPa s for D_2O[25] were used for the calculation of the hydrodynamic radius according to the Stokes–Einstein equation (eqn (1)). ^{13}C-NMR spectra could not be recorded because the concentration of the dispersed nanoparticles was too small and could not be increased without loss of colloidal stability.

Results and discussion

The reduction of $HAuCl_4$ with $NaBH_4$ leads to gold nanoparticles that are coordinated by the corresponding mercaptocarboxylic acid. The high affinity of sulphur for gold will lead to the coordination of the thiol group to the gold surface, with the carboxy group pointing outwards.

The DCS measurements in Fig. 1 show the hydrodynamic diameter of the nanoparticles. For the aliphatic ligands, a diameter of about 1.8 nm was obtained. The aromatic ligands in contrast lead to bigger hydrodynamic diameters (about 2–4.4 nm), probably due to their larger size which increases the particle radius. No correlation was found between the position of the thiol function at the aromatic ring and the diameter of the particles. All particles were well dispersed and agglomerated only to a small extent.

To analyse their size, shape and crystal structure, high-resolution transmission electron microscopy (HRTEM) was performed for gold nanoparticles functionalized with 6-mercaptohexanoic acid as well as for gold nanoparticles functionalized with 4-mercaptobenzoic acid (Fig. 2).

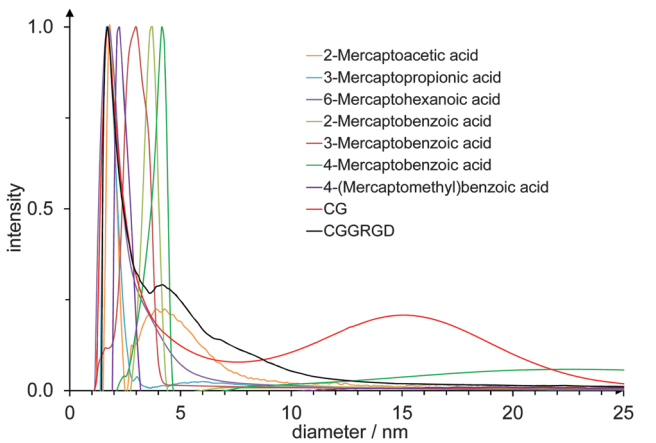

Fig. 1 DCS data of gold nanoparticles, functionalized with different mercapto-carboxylic acid ligands and two cysteine-terminated peptides.

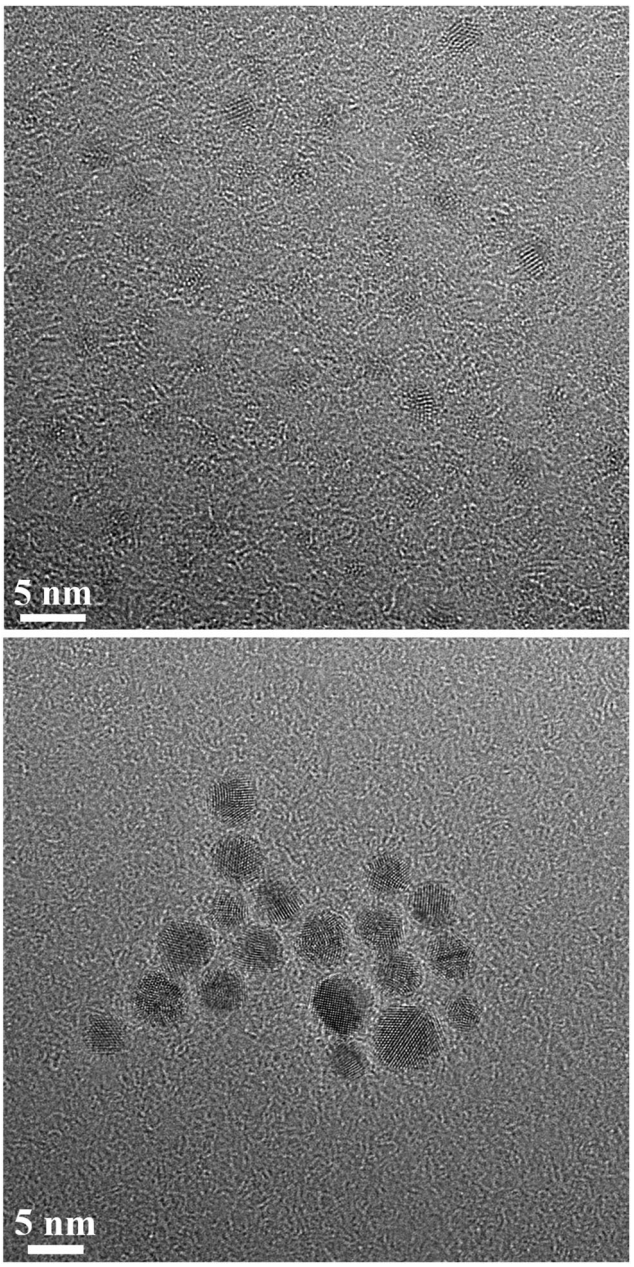

Fig. 2 High-resolution transmission electron microscopy of gold nanoparticles, functionalized with 6-mercaptohexanoic acid (top) and with 4-mercaptobenzoic acid (bottom).

For gold nanoparticles functionalized with 6-mercaptohexanoic acid, high-resolution transmission electron microscopy showed spherical particles of almost identical diameter with an average size of 1.6 ± 0.3 nm. The average size of gold nanoparticles, functionalized with 4-mercaptobenzoic acid, was 3.7 ± 0.6 nm. These numbers are in good agreement with the DCS results, despite the fact that HRTEM shows the metallic core only, and confirm that the particles are well dispersed, *i.e.* not agglomerated. A closer inspection of the nanoparticles shows that they are crystalline but typically consist of several domains. Note that the organic shell is not visible in the HRTEM images due to the low contrast with respect to the carbon background.

The diffusion coefficient of nanoparticles in solution depends on their hydrodynamic diameter. This diameter in turn depends on the effective size and shape of the particles under the given conditions (*i.e.*, temperature, solvent). If the diffusion coefficient is known, it can be used to calculate the effective size of the dispersed particles, *i.e.* the hydrodynamic diameter. In the case of a spherical particle in a homogeneous solution, the hydrodynamic diameter d_H can be computed by the Stokes–Einstein equation

$$d_H = \frac{k_B T}{3\pi\eta D} \quad (1)$$

where k_B is the Boltzmann constant, T is the temperature, η is the viscosity of the medium, and D is the self-diffusion coefficient. Larger particles diffuse more slowly in a given solvent and have a lower self-diffusion coefficient in comparison to smaller particles. The DOSY experiment gives a time-averaged diffusion rate where small anisotropies in the particle shape are averaged.

The mercaptocarboxylic acid ligands were studied using ^{1}H-NMR spectroscopy in pure form and after conjugation to the gold nanoparticles. We will discuss each compound separately in the following. All ligands and the main results are summarized in Table 1.

2-Mercaptoacetic acid

This compound has the simplest structure of all ligands used. In principle, only one signal is expected in the ^{1}H-NMR spectrum for the methylene group, assuming a rapid exchange of the carboxylic acid proton and the thiol proton in the solvent. This was indeed the case for the pure dissolved ligand. Surprisingly, after the coordination of 2-mercaptoacetic acid to a gold nanoparticle, the singlet of the α-CH_2 protons has changed into a multitude of singlet signals. Fig. 3 shows the ^{1}H-NMR spectra of the pure ligand and of the ligand coordinated to the gold nanoparticles.

The ^{1}H,^{1}H-COSY spectrum (Fig. 4) shows that there are no couplings between the major resonances, *i.e.* the sample contains a considerable number of magnetically independent molecules. Obviously, the contact to the gold nanoparticle has shifted the methylene signal downfield and, presumably, there are different kinds of bound molecules that differ in the shift of the CH_2-signal. Each type of binding must have a considerable stability as the corresponding signals can be observed individually without significant lifetime broadening. It is difficult to envision a change in the structure of 2-mercaptoacetic acid during the coordination, therefore the increased complexity of the NMR spectrum must be due to different chemical (magnetic) environments of the same molecule.

An indication on the relative contributions can be derived from the integral values of the NMR signals: there are signals with an integral of about 2.8 and other ones with integrals around 1. This may be due to two different conformations of the molecule in a 1 : 2.8 molar ratio.

The ^{1}H-DOSY spectrum (Fig. 4) shows that these different hydrogen-containing compounds have almost the same diffusion coefficient. Using the Stokes–Einstein equation, this diffusion

Table 1 The thiol-terminated ligands used for the functionalization of gold nanoparticles and the results of DCS and DOSY

		Functionalized gold nanoparticles		
Ligand	Structure	Hydrodynamic diameter (DCS)/nm	Diffusion coefficient (DOSY)/m^2 s^{-1}	Hydrodynamic diameter (DOSY)/nm
2-Mercaptoacetic acid	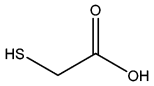	1.8	2.3×10^{-10}	1.7
3-Mercaptopropionic acid	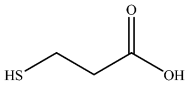	1.7	1.9×10^{-10}	2.0
6-Mercaptohexanoic acid	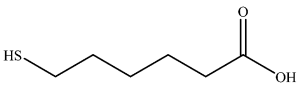	1.7	1.5×10^{-10}	2.7
2-Mercaptobenzoic acid	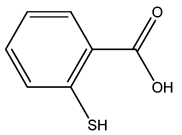	3.7	3.6×10^{-10}	1.1
3-Mercaptobenzoic acid	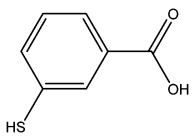	3.0	1.3×10^{-10}	3.1
4-Mercaptobenzoic acid	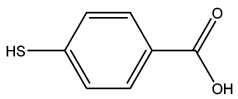	4.2	0.91×10^{-10}	4.4
Dipeptide CG	Cys–Gly	1.7	0.98×10^{-10}	4.0
Hexapeptide CGGRGD	Cys–Gly–Gly–Arg–Gly–Asp	1.7	1.19×10^{-10}	3.4

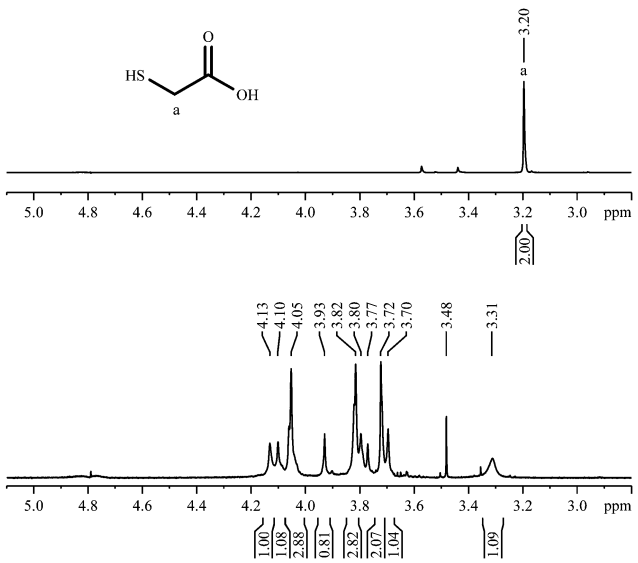

Fig. 3 ^{1}H-NMR spectra of 2-mercaptoacetic acid, pure (top; 300 MHz) and coordinated to gold nanoparticles (bottom; 600 MHz).

coefficient leads to a hydrodynamic diameter of about 1.7 nm. This corresponds very well to the DCS data (1.8 nm; Table 1). The fact that the diffusion coefficient is identical for all signals confirms that all proton-containing compounds are actually coordinated to the nanoparticle surface and not just dissolved impurities or dissociated ligand molecules.

3-Mercaptopropionic acid

3-Mercaptopropionic acid shows two triplets for adjacent methylene groups in the ^{1}H-NMR spectrum (Fig. 5). Again, additional signals appear when the ligand is coordinated to the gold nanoparticle. The small triplets at about 2.80 and 2.88 ppm belong to residual of the corresponding disulphide (3,3′-dithiodipropionic acid).

Fig. 6 shows the ^{1}H,^{1}H-COSY spectrum where the signals at 3.37 ppm and 3.63 ppm exhibit cross peaks with the signals at 2.70–2.90 ppm. However, no cross peaks are detected between the signals at 3.37 ppm and 3.63 ppm. So presumably we deal with two different species on the particle surface, each responsible for a contribution to the group of signals at 2.75 ppm, but differing in the chemical shift above 3 ppm. From the integral values (Fig. 5), the molar ratio can be estimated to be around 1 : 2.

According to the DOSY-spectrum, both components are connected to the particle surface as they move with the same diffusion coefficient. This gives a hydrodynamic diameter of about 2.0 nm that is in good agreement with the results of the DCS (1.7 nm).

6-Mercaptohexanoic acid

6-Mercaptohexanoic acid shows four signals in the ^{1}H-NMR spectrum (Fig. 7). The small signal at 2.14 ppm is due to residual acetone. The spectrum of the coordinated ligand shows additional broadened signals, despite the measurement using

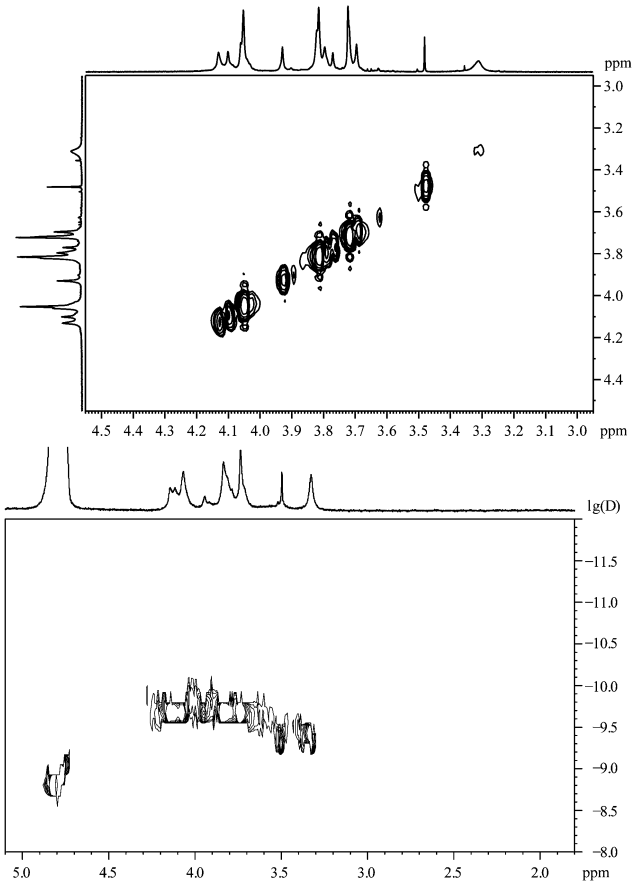

Fig. 4 2-Mercaptoacetic acid, coordinated to gold nanoparticles. Top: ^{1}H,^{1}H-COSY spectrum. Bottom: the ^{1}H-DOSY spectrum with the chemical shift in ppm against lg(*D*).

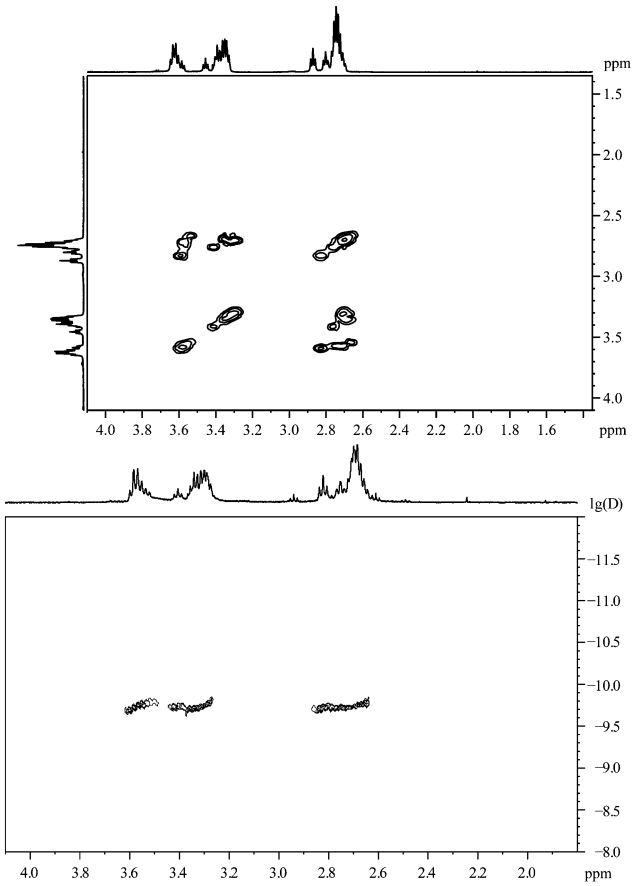

Fig. 6 3-Mercaptopropionic acid, coordinated to gold nanoparticles. Top: the ^{1}H,^{1}H-COSY spectrum. Bottom: the ^{1}H-DOSY spectrum with the chemical shift in ppm against lg(*D*).

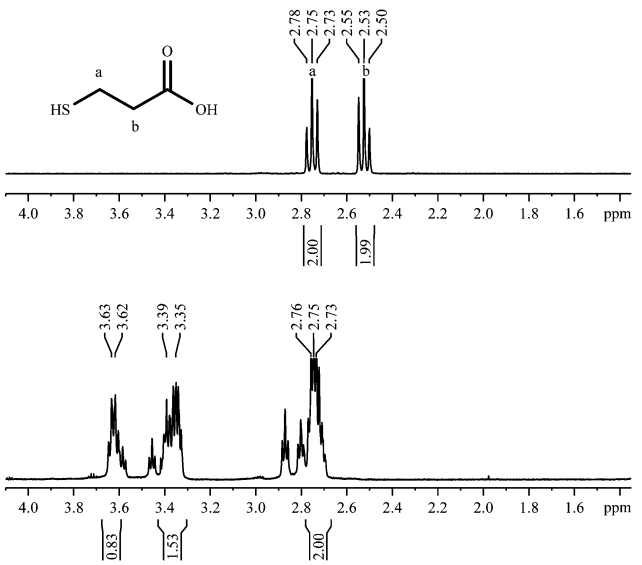

Fig. 5 ^{1}H-NMR spectra of 3-mercaptopropionic acid, pure (top; 300 MHz) and coordinated to gold nanoparticles (bottom; 600 MHz).

a 600 MHz spectrometer. As seen before with 3-mercaptopropionic acid (Fig. 5), there are two signals at a higher chemical shift that belong to the CH_2-group next to the thiol group. On the other hand, the signal at 2.22 ppm appears to be less broadened. According to the COSY spectrum, this signal belongs to the α-CH_2-group which is most distant from the nanoparticle. This confirms an adsorption by the thiol group, with the carboxylic group pointing outwards into the water.

The ^{1}H,^{1}H-COSY spectrum (Fig. 8) resembles the COSY-spectrum of 3-mercaptopropionic acid (Fig. 6). The signals at 3.41 and 3.14 ppm show cross peaks with the signal at 1.88 ppm. However, there are no cross peaks between the signals at 3.41 ppm and 3.14 ppm or between the peak at 1.61 ppm and signals above 3 ppm. This is again a strong indication for the presence of different environments for the adsorbed molecules.

According to the DOSY-spectrum, all varieties of adsorbed molecules are connected to the particle surface as they move with the same diffusion coefficient. This gives a hydrodynamic diameter of about 2.7 nm, *i.e.* about 1 nm larger than the diameter found by DCS. The diameter of the metallic core determined by TEM was 1.6 nm.

2-Mercaptobenzoic acid

Aromatic ligands have less conformational flexibility than aliphatic ligands. Therefore, we have prepared gold nanoparticles

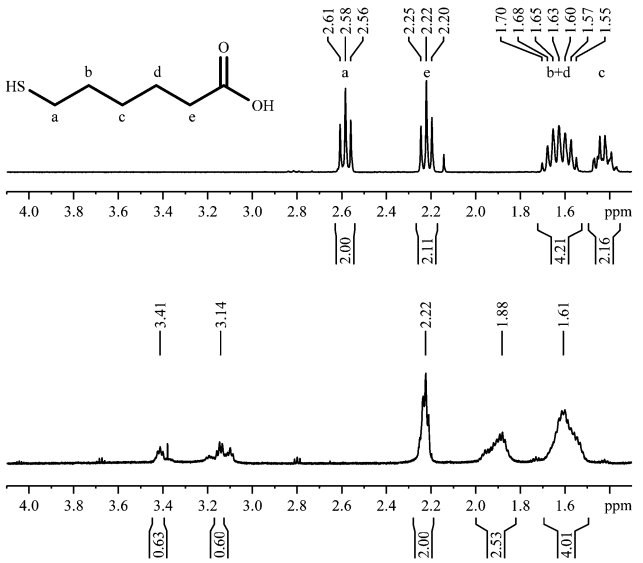

Fig. 7 ^{1}H-NMR spectra of 6-mercaptohexanoic acid, pure (top; 300 MHz) and coordinated to gold nanoparticles (bottom; 600 MHz).

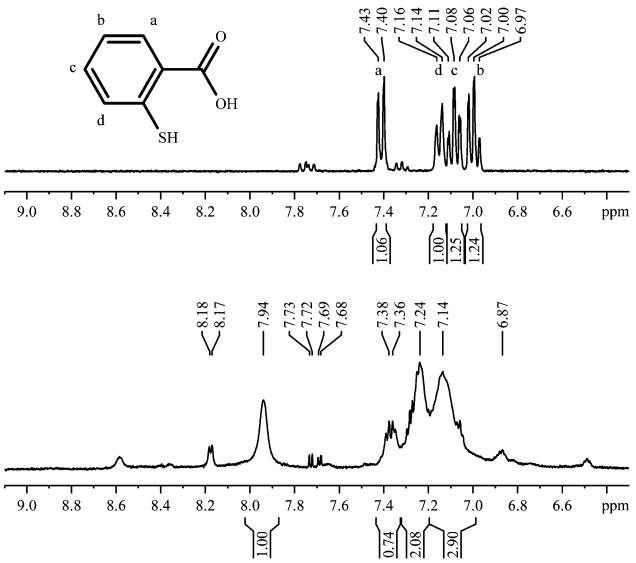

Fig. 9 ^{1}H-NMR spectra of 2-mercaptobenzoic acid, pure (top; 300 MHz) and coordinated to gold nanoparticles (bottom; 600 MHz).

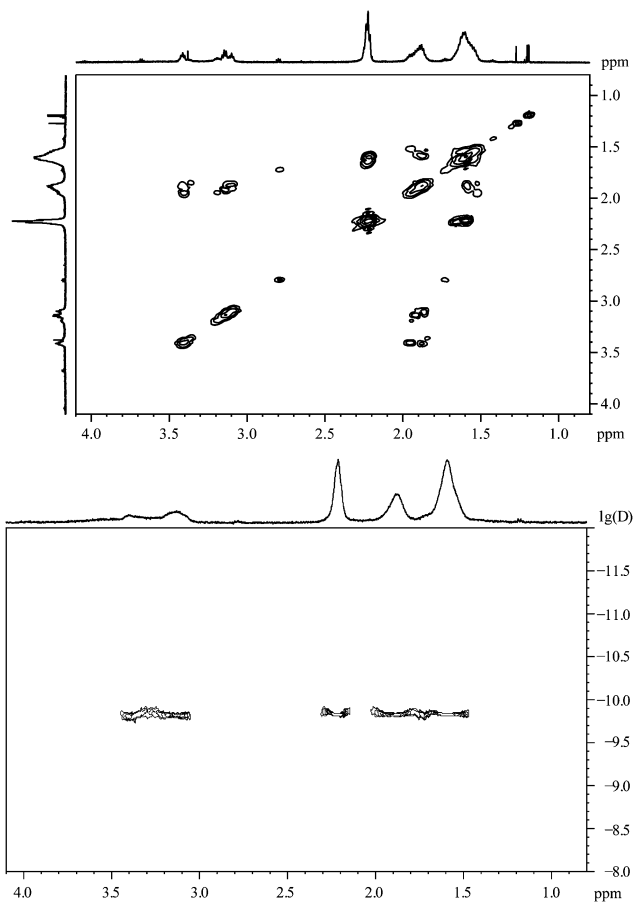

Fig. 8 6-Mercaptohexanoic acid, coordinated to gold nanoparticles. Top: the ^{1}H,^{1}H-COSY spectrum. Bottom: the ^{1}H-DOSY spectrum with the chemical shift in ppm against lg(*D*).

with the three isomeric mercaptobenzoic acids. Fig. 9 shows the ^{1}H-NMR spectra of 2-mercaptobenzoic acid. Again, there are more and broadened signals for the coordinated ligand compared to the free ligand.

The ^{1}H,^{1}H-COSY spectrum of nanoparticles capped with 2-mercaptobenzoic acid shows a poor signal-to-noise ratio (Fig. 10). Many cross peaks can be found but some of them are not symmetric to the diagonal of the spectrum.

The ^{1}H-DOSY spectrum of 2-mercaptobenzoic acid-functionalized gold nanoparticles confirms that all organic molecules are attached to the gold nanoparticles. In this case, the hydrodynamic diameter of about 1.1 nm from DOSY is significantly lower than the value obtained from DCS measurements (3.7 nm).

3-Mercaptobenzoic acid

The spectrum of 3-mercaptobenzoic acid shows a similar picture with broadened peaks, shifted downfield (Fig. 11).In contrast to 2-mercaptobenzoic acid, the meta-isomer shows only one intense cross peak in the ^{1}H,^{1}H-COSY spectrum (Fig. 12).

The ^{1}H-DOSY spectrum gives a hydrodynamic diameter of 3.1 nm in good agreement with the value from DCS (3.0 nm), again with all species on the nanoparticle surface.

4-Mercaptobenzoic acid

The *para* isomer shows a particularly simple NMR spectrum and offers no conformational degrees of freedom. The ^{1}H-NMR spectrum shows broad signals indicating the presence of nanoparticles (Fig. 13). The sharp signals at 7.67 ppm and 7.86 ppm belong to the corresponding disulphide that could not be fully removed by extraction with diethylether or toluene. Both sets of aromatic protons are shifted upfield and significantly broadened, but still in the same distance.

Fig. 14 shows the ^{1}H,^{1}H-COSY spectrum of the gold nanoparticles capped with 4-mercaptobenzoic acid. The cross peak between the broad signals is not symmetric to the diagonal of the spectrum.

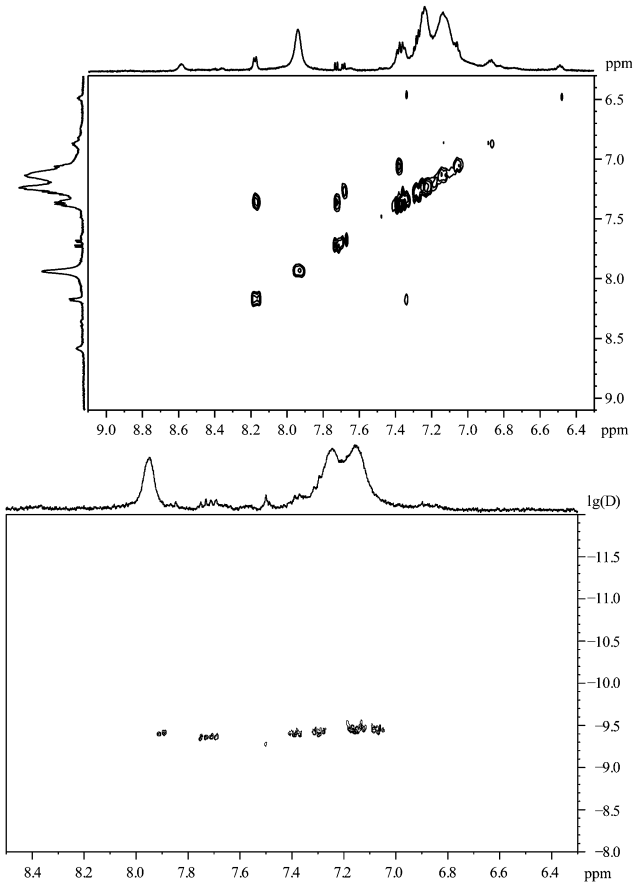

Fig. 10 2-Mercaptobenzoic acid, coordinated to gold nanoparticles. Top: the ^{1}H,^{1}H-COSY spectrum. Bottom: the ^{1}H-DOSY spectrum with the chemical shift in ppm against lg(*D*).

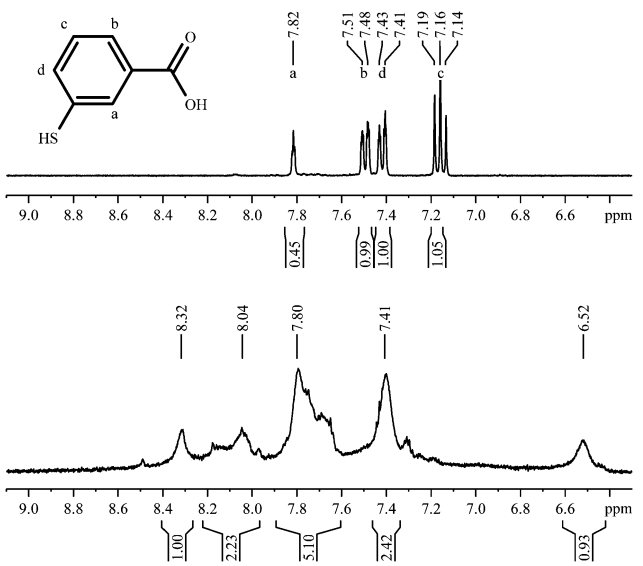

Fig. 11 ^{1}H-NMR spectra of 3-mercaptobenzoic acid, pure (top; 300 MHz) and coordinated to gold nanoparticles (bottom; 600 MHz).

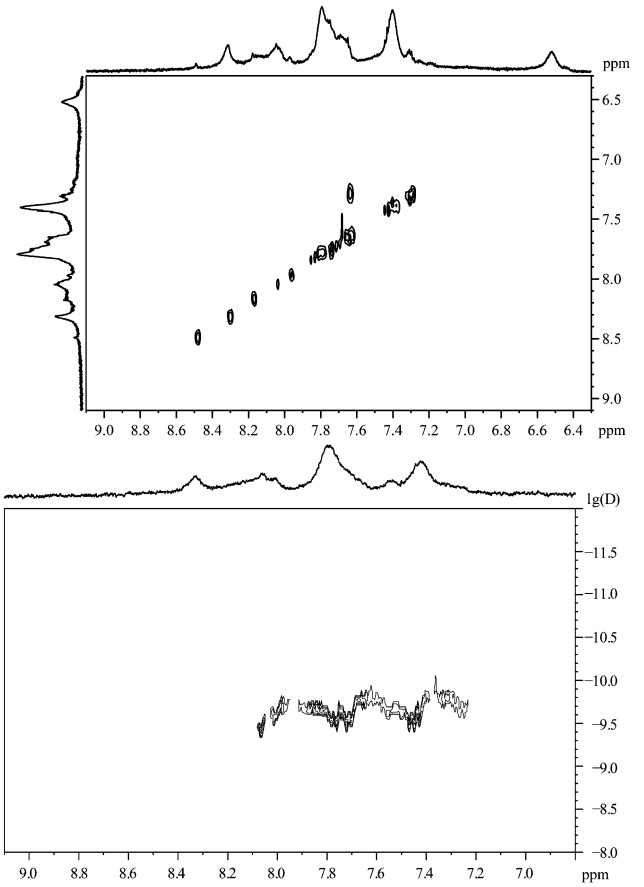

Fig. 12 3-Mercaptobenzoic acid, coordinated to gold nanoparticles. Top: the ^{1}H,^{1}H-COSY spectrum. Bottom: the ^{1}H-DOSY spectrum with the chemical shift in ppm against lg(*D*).

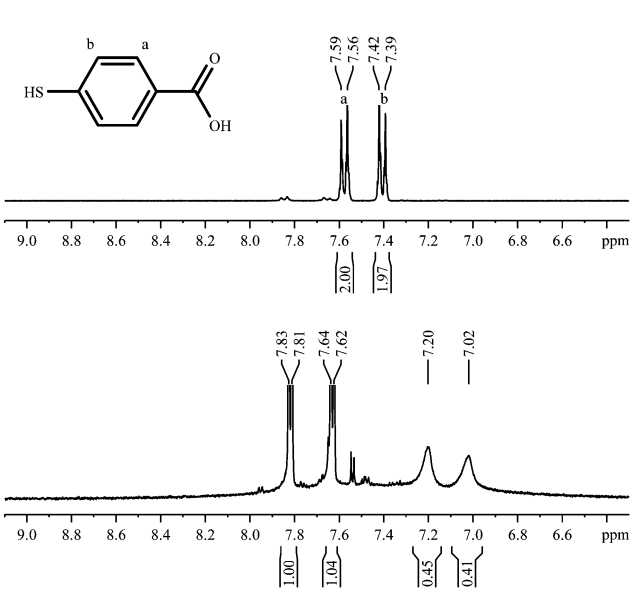

Fig. 13 ^{1}H-NMR spectra of 4-mercaptobenzoic acid, pure (top; 300 MHz) and coordinated to gold nanoparticles (bottom; 600 MHz).

The ^{1}H-DOSY spectrum (Fig. 14) of the gold nanoparticles, capped with 4-mercaptobenzoic acid, shows that all particles have the same diffusion coefficient with a hydrodynamic diameter of 4.4 nm, in good agreement with the DCS results (4.2 nm) and HRTEM results (3.7 nm; metallic core).

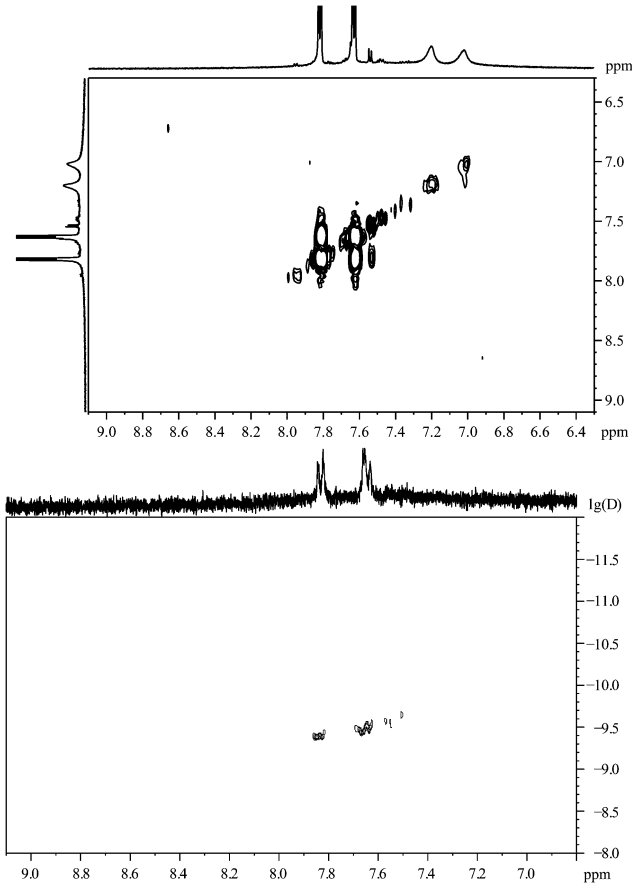

Fig. 14 4-Mercaptobenzoic acid, coordinated to gold nanoparticles. Top: the ^{1}H,^{1}H-COSY spectrum. Bottom: the ^{1}H-DOSY spectrum with the chemical shift in ppm against lg(*D*).

The Cys–Gly dipeptide

As gold nanoparticles are often used to carry biomolecules, the attachment of peptides was performed. As a linker group, we used the thiolated amino acid cysteine (Cys or C). The ^{1}H-NMR spectrum of the dipeptide cysteine–glycine shows three signals and a full H/D exchange of carboxy-, amino- and thiol-protons (Fig. 15). Due to the suppression of the water signal by proton decoupling, the integral of the signal at 4.24 is smaller than it should be. The resulting spectrum of the dipeptide coordinated to the nanoparticles shows a multitude of broadened signals, typically shifted downfield.

The ^{1}H,^{1}H-COSY spectrum of the dipeptide attached to gold nanoparticles is shown in Fig. 16. No cross peaks can be found although the aliphatic protons of the cysteine should lead to a vicinal coupling.

The diffusion coefficient measured by ^{1}H-DOSY is in accordance with a hydrodynamic diameter of about 4.0 nm. In the spectrum, one component can be found with a higher diffusion coefficient than the other signals. That means that the compound with a chemical shift of 3.67 ppm (sharp peak) is not attached to the particles but dissolved.

The hexapeptide CGGRGD

As a more relevant biomolecule, the prominent RGD sequence was attached to the gold nanoparticle surface with a diglycine spacer and a cysteine linker. In Fig. 17, the NMR spectra of the peptide CGGRGD are shown. The signal of the α-proton of the

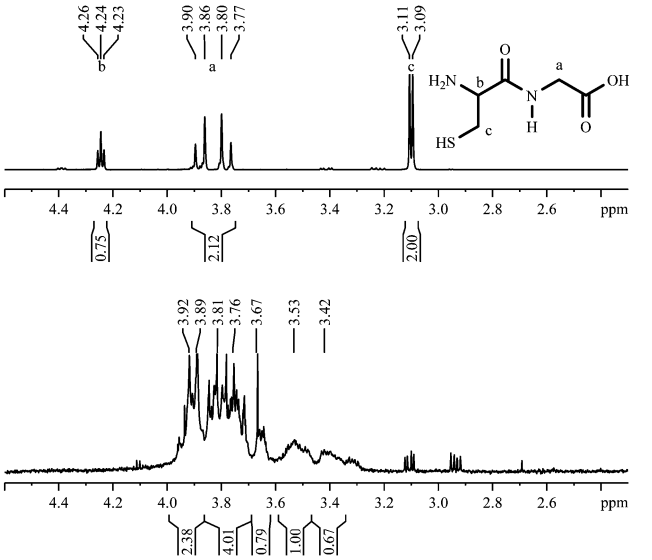

Fig. 15 ^{1}H-NMR spectra of Cys–Gly, dissolved (top; 300 MHz) and coordinated to gold nanoparticles (bottom; 600 MHz).

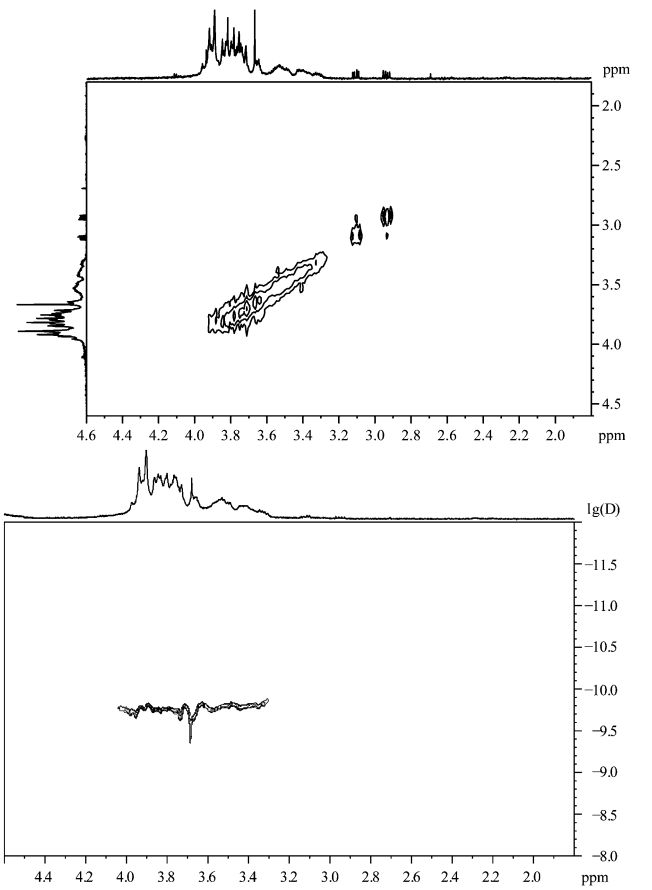

Fig. 16 Cys–Gly, coordinated to gold nanoparticles. Top: the ^{1}H,^{1}H-COSY spectrum. Bottom: the ^{1}H-DOSY spectrum with the chemical shift in ppm against lg(*D*).

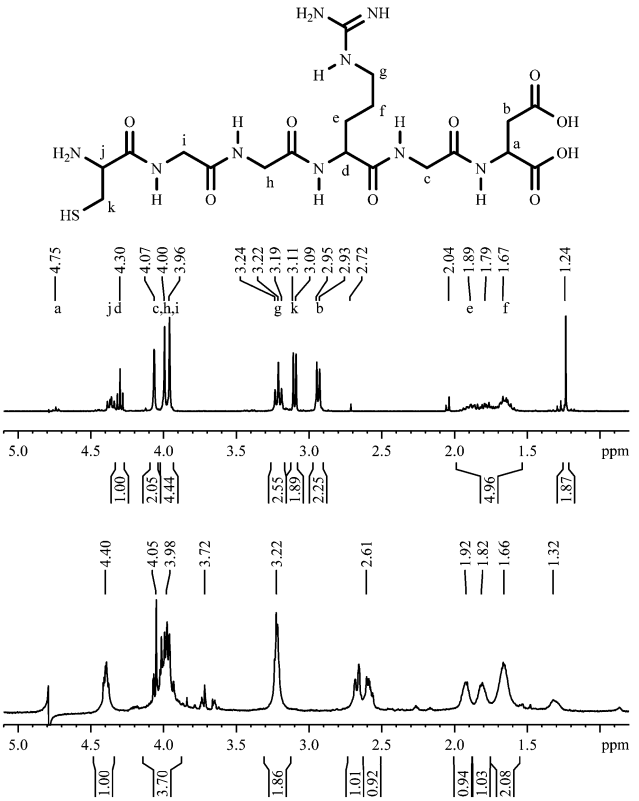

Fig. 17 ^{1}H-NMR spectra CGGRGD, pure (top; 300 MHz) and coordinated to gold nanoparticles (bottom; 600 MHz).

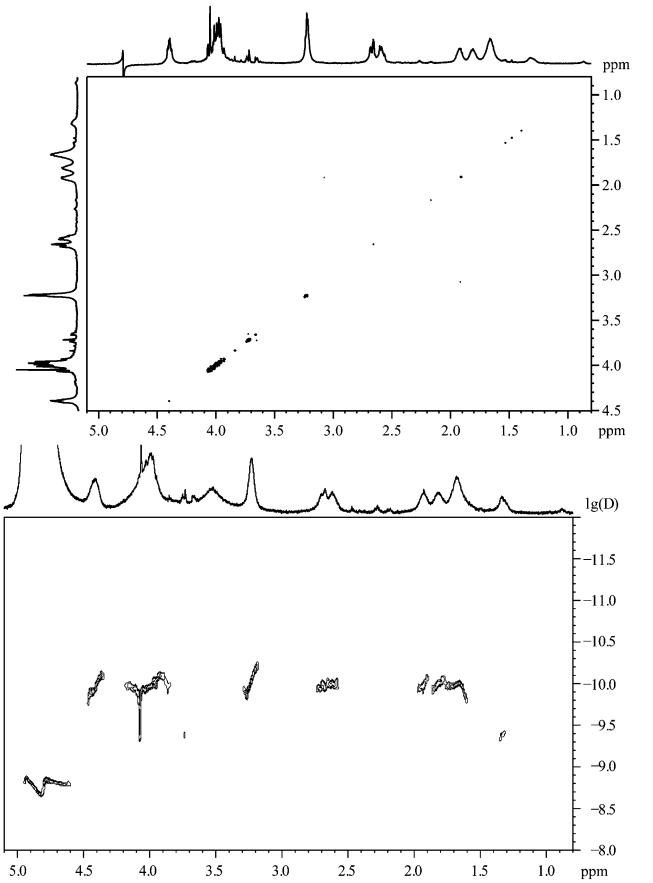

Fig. 18 The hexapeptide CGGRGD, coordinated to gold nanoparticles. Top: the ^{1}H,^{1}H-COSY spectrum. Bottom: the ^{1}H-DOSY spectrum with the chemical shift in ppm against lg(*D*).

asparagine is very small due to the suppression of the water signal by proton decoupling with composite pulses. The signal at 1.24 ppm belongs to an unknown impurity in the delivered peptide. Again, after the attachment to the gold nanoparticles all signals are broadened and shifted. No conclusions are possible with respect to the orientation of the hexapeptide.

In Fig. 18 the ^{1}H–^{1}H-COSY spectrum of nanoparticles stabilized by the hexapeptide CGGRGD is shown. Like in the spectrum of the dipeptide, no cross peaks can be found although several ^{3}J-couplings are expected.

The ^{1}H-DOSY spectrum of the nanoparticles capped with the hexapeptide CGGRGD is similar to the spectrum of CG as shown above (Fig. 16). A compound with a smaller diffusion coefficient can be found indicating a species not attached to the particle. Like with the dipeptide, there is a discrepancy between the values of DCS (1.7 nm) and the DOSY leading to a hydrodynamic diameter of about 3.4 nm.

Summarizing, it can be stated that ^{1}H-NMR spectroscopy is possible on ligands that are attached to ultrasmall gold nanoparticles. However, the ^{1}H-NMR spectra of the coordinated ligands are much more complex than the spectra of the dissolved pure ligands. All proton signals are broadened as well as shifted with respect to the spectra of the same molecules in solution. Similar observations have been made on multiple occasions, as reported by Volkert *et al.*[10] As expected, the variation of the shift generally increases with decreasing distance between the gold surface and the observed spin.

For all ligands included in this study we found that the number of peaks strongly increases and that most of them are shifted downfield. Together with the signal widening, this makes a clear structural assignment almost impossible. A chemical change of the ligands during the coordination can be ruled out almost with certainty under the synthesis conditions; therefore the complex spectra must be caused by the vicinity of the metallic nanoparticle that leads to different chemical environments and chemical shifts for the same molecule, possibly depending on its orientation on a specific crystallographic surface.

It is well known that metallic nanoparticles will cause a dipolar magnetic interaction with the proton spins of the adsorbed organic molecules. This interaction varies with the distance and the angular orientation of the proton *vs.* the particle centre and the external magnetic field. Therefore, it is partially averaged by conformational and diffusive reorientation.[22,26] Based on the expected rotational diffusion for particles of a diameter of 1.8 nm, the observed line broadening of the observed proton signals is surprisingly small, especially in the case of the spectrum of 3-mercaptopropionic acid (Fig. 5). For the other aliphatic carboxylic acids, the observed widening seems to rather be related to complex splitting patterns than to dynamic broadening (Fig. 7 and 9). The discrepancy becomes obvious

when the proton signals a and b of 3-mercaptopropionic acid are compared with the corresponding proton and carbon signals of 1-octanethiol[22] or 1-dodecanthiol[19] bound to gold clusters of similar size. Obviously, the aliphatic carboxylic acids in the aqueous environment retain a significant degree of conformational freedom even when connected to the particle surface, leading to an efficient pre-averaging of the dipolar interaction. For 11-mercaptoundecanoic acid, bound to silver–gold nanoparticles (70 : 30) with a diameter of 1.8 nm, we have also found broadened peaks, but with a smaller downfield shift than in these cases. This may be due to the longer alkyl chain which extends into water where the protons are less influenced when they are in a greater distance from the metallic nanoparticle.[20]

In contrast, the aromatic carboxylic acids show significant dynamic broadening, especially for the signals around 7 ppm of 4-mercaptobenzoic acid (Fig. 13). In accordance with the explanation given above, this may be a consequence of the conformational rigidity of the aromatic group.

Diffusion ordered NMR spectroscopy (DOSY) can serve as a valuable tool for the determination of the hydrodynamic radius of particles *via* the measurement of the self-diffusion constant in an environment of known viscosity.[24] More importantly, it is a safe indicator for the binding state of the observed ligands. The fact that all ligand protons reflect the diffusion behaviour of the gold particles clearly shows that the ligand is constantly bound to the particle surface. Obviously, neither free ligand molecules nor larger clusters of coated gold particles (which would have a higher hydrodynamic radius) occur in the samples. This also excludes an exchange of ligand molecules between particles by free diffusion, as even brief periods of free diffusion would largely affect the averaged diffusion rate and therefore show up in the DOSY spectrum.

Conclusions

NMR spectroscopy is a useful tool to analyse inorganic nanoparticles in dispersion, especially to determine the hydrodynamic particle size by ^{1}H-DOSY. In all spectra of coordinated molecules, we found additional signals which generally had higher chemical shifts and indicate the presence of multiple molecular species of ligand molecules. Interestingly, these different species are all attached to the gold nanoparticles as the DOSY spectra clearly prove. As a chemical change of these ''simple'' molecules can most likely be ruled out, we conclude that there are (conformational? crystallographic?) effects that influence the proton NMR spectra that are not yet understood, but constitute a general phenomenon that deserves further attention. The binding of cysteine-containing peptides to gold nanoparticles can be demonstrated by NMR spectroscopy, opening up the possibility for a better understanding of the interaction of receptor-coated gold nanoparticles with larger biomolecules like proteins or even with cell surfaces.

Acknowledgements

We thank Manfred Zaehres for the opportunity of the measurements of the ^{1}H-DOSY spectra. Heinz Bandmann is thanked for the measurements of the spectra at the 600 MHz spectrometer. M. E. thanks the Deutsche Forschungsgemeinschaft (DFG) for funding within the framework of the Collaborative Research Center SFB 1093. M. H and M. G. thank the Deutsche Forschungsgemeinschaft (DFG) for support within the grant HE 7192/1-1.

Notes and references

1 G. Schmid, *Nanoparticles. From Theory to Application*, Wiley-VCH, Weinheim, 2004.
2 R. A. Sperling, P. Rivera, F. Zhang, M. Zanella and W. J. Parak, *Chem. Soc. Rev.*, 2008, **37**, 1896–1908.
3 E. C. Dreaden, A. M. Alkilany, X. Huang, C. J. Murphy and M. A. El-Sayed, *Chem. Soc. Rev.*, 2012, **41**, 2740–2779.
4 D. A. Giljohann, D. S. Seferos, W. L. Daniel, M. D. Massich, P. C. Patel and C. A. Mirkin, *Angew. Chem., Int. Ed.*, 2010, **49**, 3280–3294.
5 R. Sardar, A. M. Funston, P. Mulvaney and R. W. Murray, *Langmuir*, 2009, **25**, 13840–13851.
6 D. Mahl, C. Greulich, W. Meyer-Zaika, M. Köller and M. Epple, *J. Mater. Chem.*, 2010, **20**, 6176–6181.
7 M. Brust, M. Walker, D. Bethell, D. J. Schiffrin and R. Whyman, *Chem. Commun.*, 1994, 801–802.
8 M. Homberger and U. Simon, *Philos. Trans. R. Soc., A*, 2010, **368**, 1405–1453.
9 A. Leifert, Y. Pan-Bartnek, U. Simon and W. Jahnen-Dechent, *Nanoscale*, 2013, **5**, 6224–6242.
10 A. A. Volkert, V. Subramaniam, M. R. Ivanov, A. M. Goodman and A. J. Haes, *ACS Nano*, 2011, **5**, 4570–4580.
11 C. Rehbock, J. Jakobi, L. Gamrad, S. van der Meer, D. Tiedemann, U. Taylor, W. Kues, D. Rath and S. Barcikowski, *Beilstein J. Nanotechnol.*, 2014, **5**, 1523–1541.
12 A. Neumeister, J. Jakobi, C. Rehbock, J. Moysig and S. Barcikowski, *Phys. Chem. Chem. Phys.*, 2014, **16**, 23671–23678.
13 N. Li, P. Zhao, L. Salmon, J. Ruiz, M. Zabawa, N. S. Hosmane and D. Astruc, *Inorg. Chem.*, 2013, **52**, 11146–11155.
14 A. Badia, W. Gao, S. Singh, L. Demers, L. Cuccia and L. Reven, *Langmuir*, 1996, **12**, 1262–1269.
15 A. Badia, S. Singh, L. Demers, L. Cuccia, G. R. Brown and R. B. Lennox, *Chem. – Eur. J.*, 1996, **2**, 359–363.
16 A. Badia, L. Demers, L. Dickinson, F. G. Morin, R. B. Lennox and L. Reven, *J. Am. Chem. Soc.*, 1997, **119**, 11104–11105.
17 Y. Song, A. S. Harper and R. W. Murray, *Langmuir*, 2005, **21**, 5492–5500.
18 A. Dass, R. Guo, J. B. Tracy, R. Balasubramanian, A. D. Douglas and R. W. Murray, *Langmuir*, 2008, **24**, 310–315.
19 M. J. Hostetler, J. E. Wingate, C. J. Zhong, J. E. Harris, R. W. Vachet, M. R. Clark, J. D. Londono, S. J. Green, J. J. Stokes, G. D. Wignall, G. L. Glish, M. D. Porter, N. D. Evans and R. W. Murray, *Langmuir*, 1998, **14**, 17–30.
20 S. Ristig, D. Kozlova, W. Meyer-Zaika and M. Epple, *J. Mater. Chem. B*, 2014, **2**, 7887–7895.
21 J. S. Seo, D. M. Son, H. Lee, J. Kim and Y. Kim, *Bull. Korean Chem. Soc.*, 2009, **30**, 2651–2654.

22 R. H. Terrill, T. A. Postlethwaite, C. H. Chen, C. D. Poon, A. Terzis, A. Chen, J. E. Hutchison, M. R. Clark and G. Wignall, *J. Am. Chem. Soc.*, 1995, **117**, 12537–12548.
23 D. A. Fleming, C. J. Thode and M. E. Williams, *Chem. Mater.*, 2006, **18**, 2327–2334.
24 K. Salorinne, T. Lahtinen, J. Koivisto, E. Kalenius, M. Nissinen, M. Pettersson and H. Häkkinen, *Anal. Chem.*, 2013, **85**, 3489–3492.
25 F. J. Millero, R. Dexter and E. Hoff, *J. Chem. Eng. Data*, 1971, **16**, 85–87.
26 A. Terheiden and C. Mayer, *Phase Trans.*, 2004, **77**, 81–87.